Plasmon-based photopolymerization: near-field probing, advanced photonic nanostructures and nanophotochemistry

2014 J. Opt. 16 114002

(http://iopscience.iop.org/2040-8986/16/11/114002)

OPEN ACCESS
IOP Publishing
Journal of Optics
J. Opt. **16** (2014) 114002 (17pp)
doi:10.1088/2040-8978/16/11/114002

Review

Plasmon-based photopolymerization: near-field probing, advanced photonic nanostructures and nanophotochemistry

Xuan Zhou[1], Olivier Soppera[2], Jérôme Plain[1], Safi Jradi[1], Xiao Wei Sun[3], Hilmi Volkan Demir[3,5], Xuyong Yang[3], Claire Deeb[1,6], Stephen K Gray[4], Gary P Wiederrecht[4] and Renaud Bachelot[1]

[1] Institut Charles Delaunay-Laboratoire de Nanotechnologie et d'Instrumentation Optique (ICD-LNIO), CNRS UMR 6281, Université de Technologie de Troyes, Troyes, France
[2] Institut de Science des Matériaux de Mulhouse IS2M, CNRS UMR 7361, Université de Haute-Alsace, Mulhouse, France
[3] LUMINOUS! Center of Excellence for Semiconductor Lighting and Displays, School of Electrical and Electronic Engineering, Nanyang Technological University, 639798, Singapore
[4] Center for Nanoscale Materials, Argonne National Laboratory, Argonne, IL 60439, USA
[5] Department of Electrical and Electronics Engineering, Bilkent University, Bilkent, Ankara TR-06800 Turkey

E-mail: renaud.bachelot@utt.fr

Received 12 August 2014, revised 9 September 2014
Accepted for publication 12 September 2014
Published 3 November 2014

Abstract

Hybrid nanomaterials are targeted by a rapidly growing group of nanooptics researchers, due to the promise of optical behavior that is difficult or even impossible to create with nanostructures of homogeneous composition. Examples of important areas of interest include coherent coupling, Fano resonances, optical gain, solar energy conversion, photocatalysis, and nonlinear optical interactions. In addition to the coupling interactions, the strong dependence of optical resonances and damping on the size, shape, and composition of the building blocks provides promise that the coupling interactions of hybrid nanomaterials can be controlled and manipulated for a desired outcome. Great challenges remain in reliably synthesizing and characterizing hybrid nanomaterials for nanooptics. In this review, we describe the synthesis, characterization, and applications of hybrid nanomaterials created through plasmon-induced photopolymerization. The work is placed within the broader context of hybrid nanomaterials involving plasmonic metal nanoparticles and molecular materials placed within the length scale of the evanescent field from the metal surface. We specifically review three important applications of free radical photopolymerization to create hybrid nanoparticles: local field probing, photoinduced synthesis of advanced hybrid nanoparticles, and nanophotochemistry.

[6] Current address: Department of Chemistry, Northwestern University 2145 Sheridan Road, Evanston, IL 60208 USA.

Keywords: nanoplasmonics, free-radical photopolymerization, nanophotochemistry, hybrid plasmonics

(Some figures may appear in colour only in the online journal)

1. Introduction

Localized surface plasmons (LSPs) are quanta of energy associated with collective oscillation of electrons in metal nanoparticles [1]. In the case of interaction with light, the rich angular spectrum of plane waves resulting from diffraction by small objects makes possible the LSP–light coupling. This coupling results in single photonic sources and radiation presenting, in particular, local field enhancement and extremely confined evanescent waves. When coupled with an external system (molecules, semiconductor quantum dots (QDs), etc), the LSP energy transfer and related Einstein coefficient (i.e. probabilities of events: rates of absorption, transition, emission, etc) can be either radiative or non-radiative. Weak or strong coupling is then possible [2]. In the case of weak coupling, energy transfer is slower than intrinsic damping or relaxation of the different involved excited states. The Purcell effect, which predicts the way an emitter emits light inside a nanocavity (in this case the metal particle itself) [3], is an example of weak coupling. In the case of strong coupling, damping is weaker and slower than the transfer of energy, allowing the energy to go back and forth between excited states of the LSP and those of the molecular system. This effect corresponds to Rabi oscillations and can result in spectral splitting. These energy transfers have been widely studied and used for many applications including light emission [4], sensing [5] and photovoltaics [6].

Over the past ten years, LSPs have been exploited for triggering and controlling photochemical and photophysical reactions. This coupling is of weak nature in the sense that the photonic LSP energy is absorbed and directly transferred into the chemical system for triggering reactions. These reactions include free radical photopolymerization involving local photon and charge transfer and solidifying the initial liquid organic formulation. This article highlights important achievements and applications of this approach. We will show that photopolymerization can be used for probing the plasmonic near-field or for synthesizing new polymer–metal hybrid nanostructures revealing unique optical properties. In particular, incorporating active species in the polymer allows for the development of a new generation of hybrid nano emitters for potential nanophotonic applications.

The article is organized as follows. In section 2 we first describe the context and framework of this work by citing and commenting on important achievements in the hybrid plasmonics community. We emphasize the possibilities for boosting and controlling photochemical and photophysical reactions via plasmonics routes. We then introduce our approach of nanoscale plasmon-based free radical photopolymerization (section 3) and present in section 4 three important applications: (i) local field probing, (ii) photo-induced synthesis of advanced hybrid nanoparticles, and (iii) nanophotochemistry. We finally conclude in section 5 and highlight some perspectives of this work.

2. Context

Our efforts to create photopolymerized, composite metal–molecule nanostructures are motivated by the novel optical effects produced by the *physical* interactions between organic and metal nanoparticle constituents. However, as will be seen throughout the paper, this work also requires a deep understanding of the *chemistry* of the free radical polymerization reaction initiated by plasmon excitation. Such a multidisciplinary knowledge request is currently the challenge of many researchers in the nanoscience community. In this section we place our work in the context of many outstanding efforts underway worldwide to create, understand, and apply molecule–plasmon interactions at the nanoscale.

The study of the interactions between plasmons and molecules in nanostructures is a rapidly growing, multidisciplinary field [7–11]. The goals of researchers in this field can be broadly separated along the lines of those striving to achieve plasmon-induced chemical reactions, and those seeking to understand the unique properties derived from coupling interactions between plasmons and molecules. A specific motivation for pursuing either goal with nanostructures is the strong correlation between nanoparticle size, shape, and composition with optical properties. This enables an extraordinarily varied, yet precise, degree of control over the optical properties of the nanoparticle building block to target a specific interaction with the molecular building block. This hybridization approach can strongly modify the static and dynamic optical behaviors of hybrid nanostructures as compared to isolated nanoparticles. Hybridization with organic materials thus presents the basis for additional control and a greater range of modified optical behavior, as compared to isolated nanoparticles, through careful fabrication and a deep understanding of the molecule–plasmon interactions.

How does hybridization specifically enable a greater range of optical properties? What additional handles are made available to researchers to change the optical properties of the new materials? A first example is the control over the spatial distribution of the organic molecules between the metallic surface and the molecules. By means of fabrication methods that allow a precise spatial positioning of an organic material next to a plasmonic nanostructure, one can change not only the resonance of the plasmon, but also induce anisotropy in the absorption and scattering cross-section of the nanoparticle. Such an effect does not necessarily require a resonant interaction between the molecules and nanoparticle, but resonance effects can produce additional anisotropy in emission lifetime and decay pathways. A focus of our work, discussed in subsequent sections, is to induce structural anisotropy at the nanoscale to induce near-field and far-field optical anisotropies, both resonantly and nonresonantly.

A second handle is control over the spacing between the metal nanoparticle surface and molecules with resonant interactions. There have been extensive efforts in

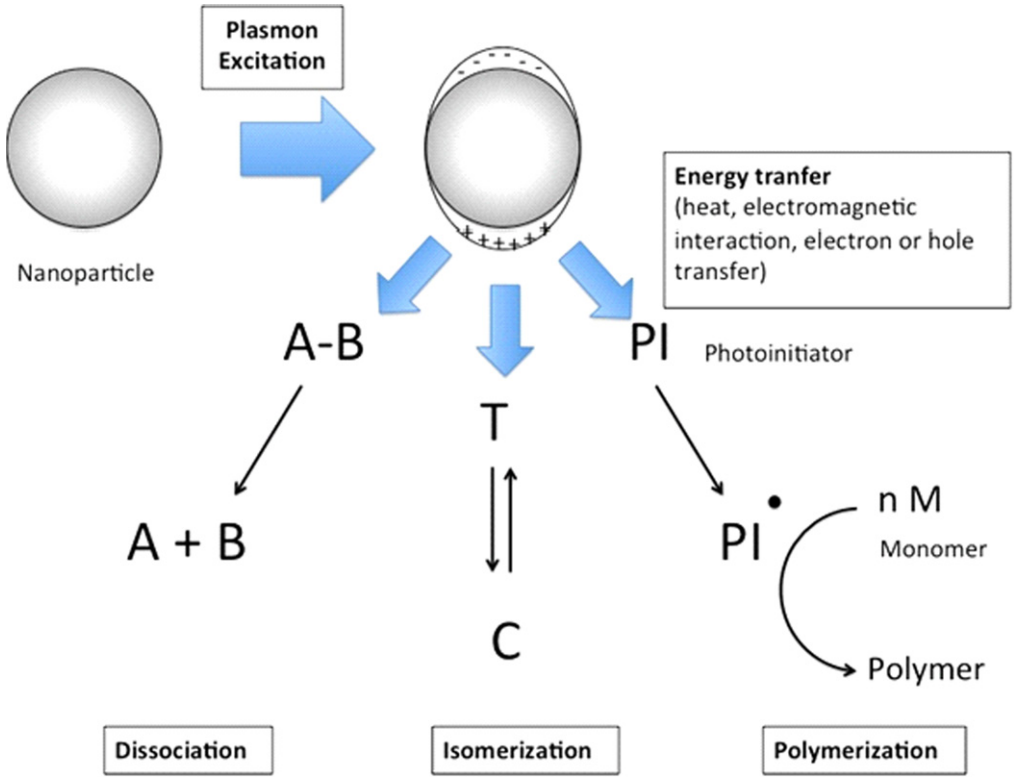

Figure 1. Primary categories of plasmon-based photoinduced chemical reactions in the context of optical near-fields.

understanding the interactions between metal surfaces and molecules, led by seminal works such those of Drexhage, Chance *et al* and Pockrand *et al* [12–14]. Many modern studies continue to explore new structures and architectures to optimize molecular and artificial molecules (QDs) responses in the evanescent fields of nanostructures [15–17]. In general, at small molecule–metal spacing, typically below 5 nm or so, there are dipole–dipole interactions that open a strong, non-radiative quenching channel following excitation. At larger spacing, radiative rates can be enhanced because of the presence of an enhanced optical near field that decays exponentially from the metal surface, while dipole–dipole interactions decay with a much higher order distance dependence.

A third handle is control over the degree of aggregation of molecular species. For example, the aggregation of molecules to form j-aggregates can produce polarizable excitons which couple strongly to surface plasmons. This has produced novel effects such as coherent coupling between plasmons and excitons, and Fano-like transparencies result [18–22].

The metal–molecule interface also plays a key role in the range of possible applications of hybrid nanostructures due to the possibility of optically-induced energy and charge migration across the interface. Additionally, the chemical nature of the interface changes with nanoparticle size and shape, once again providing control over both the degree of chemical reactivity, but also over key physical properties such as altered electronic conductivity or charge transfer at the surface of the nanoparticles [23, 24]. These observables provide clear opportunities for sensing, photocatalysis, nonlinear optics, solar energy conversion, optical gain/lasing, etc [25–31].

Within the context of these control handles, plasmon-induced photochemistry, and particularly plasmon-induced polymerization, provides a possible rational fabrication route to create hybrid nanostructures. We should note that very nice accounts and reviews of photochemistry utilizing plasmonic nanoparticles have recently appeared in the literature [28, 32, 33].

The primary plasmon-assisted chemical reactions can be classified into the three following categories, schematically illustrated in figure 1:

- Molecular dissociation.
- Photoinduced switching of photochromes.
- Photopolymerization.

The last section will focus on the applications of photopolymerization. In particular, the case of free-radical photopolymerization will be emphasized, in order to stress the specificities of the plasmon-induced photopolymerization versus far-field photopolymerization.

2.1. Plasmon-assisted chemical reactions

The first report on plasmon-enhanced photochemical reaction was provided by Chen *et al* in 1983 [34]. The photoreaction consisted of a dissociation reaction of a cadmium complex (dimethyl cadmium) on cadmium nanoparticles. The wavelength (257 nm) was chosen to overlap with the plasmon resonance of the Cd nanoparticles. Such irradiation of the Cd

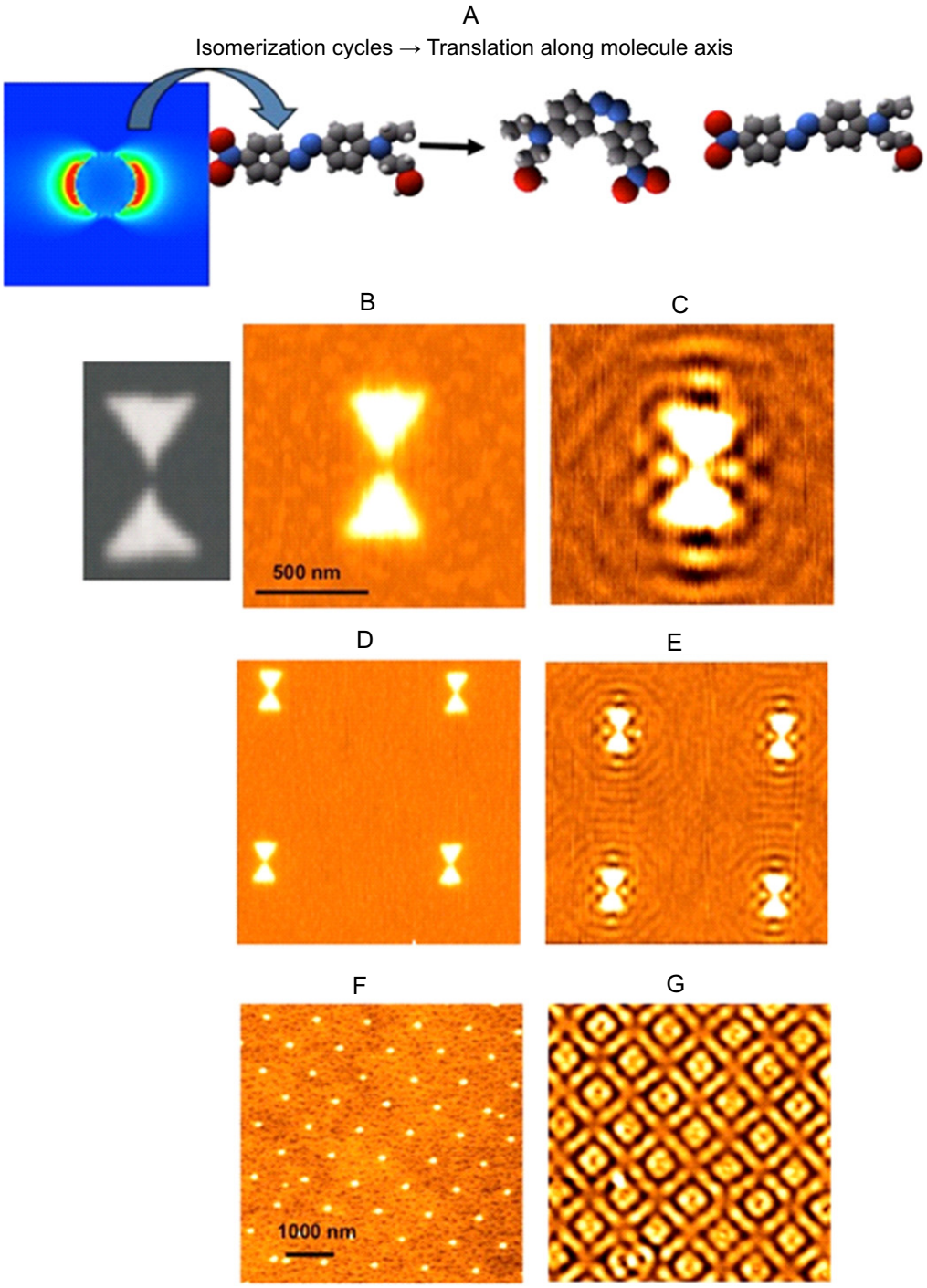

Figure 2. Near-field photochemical imaging of noble metal nanostructures using PMMA-DR1. (A) Principle: the active azobenzene molecule moves under local optical illumination. (B) AFM image of a bow–tie plasmonic antenna covered with a thin layer of PMMA-DR1 (the left image is a scanning electron micrograph of the antenna). (C) Same as (B) after optical exposure with a plane wave linearly polarized along the antenna axis. (D) and (E) Zoom out of (B) and (C). (F) AFM image of an array of silver circular nanoparticles covered with a thin layer of PMMA-DR1. (G) Same as (B) after optical exposure with a plane wave circularly polarized. (Adapted with permission from [36, 39]. Copyright 2005 American Chemical Society.)

nanoparticles in contact with the Cd complexes gave rise to elliptical nanoparticles. Following this example, many other reactions have been driven by plasmons. Other important examples of small molecules dissociation assisted by plasmons are photodissociation of alkanes on Pd nanoparticles, photodesorption of NO and site conversion of CO on Pd nanoparticles and, more recently, water splitting and photodecomposition of organic dyes on metal nanoparticles loaded on TiO_2 surfaces. Examples can be found in a recent review article from Ueno and Misawa [35].

More recently, the concept was extended to other interesting photoinduced reactions like switching of

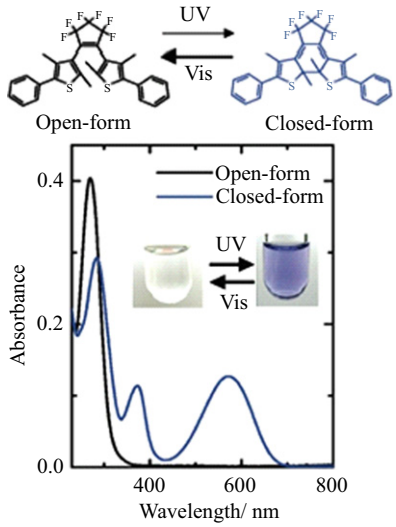

Figure 3. Molecular structure of diarylethene and spectra of open and closed forms. Reprinted with permission from [41]. Copyright 2009 American Chemical Society.

photochromes. In particular, azobenzene derivatives are known to undergo a photoinduced transition between trans and cis isomers upon visible light irradiation. This transition is reversible and can lead to the initiation of a chemical reaction by thermal and photochemical pathways. Grafting azobenzene moieties on a polymer material such as PMMA allows designing a material that can be patterned at the micro and nanoscale upon spatially controlled irradiation. This physico-chemical system has been used in different irradiation configurations and Hubert *et al* have demonstrated that it can be coupled to a metal nanoparticle surface plasmon to induce nanostructuring [36] (figure 2). In this case, the local trans–cis isomerization after photoexcitation gives rise to a mass diffusion process due to thermal reorganization and reconfiguration of the chromophores by the external electromagnetic field [37]. Such an experimental approach was used on arrays of metal nanoparticles, producing nanostructures that varied depending of the polarization of light and the metal structure. A wide variety of nanostructures geometries were used [37–40] showing that this approach is well adapted to image the near-field distribution around metal nanostructures.

Diarylethene is another class of photochromes that has been applied to optical near-field irradiation in order to generate molecular isomerization at the nanoscale. Such molecules can switch between two separate states, namely an open and a closed form. The isomerization is reversible and can be light induced (figure 3). Such systems were coupled to plasmonic nanostructures and the near-field isomerization was investigated quantitatively by Tsuboi *et al* [41]. The effect of the distance between the metal nanoparticle and the dyes was also examined [42].

A third very important example of plasmon-induced photoreaction is photopolymerization. Photopolymerization consists of forming macromolecules from monomers or mixtures of monomers by free radical or ionic reactions triggered by light. Combining the optical near-field with photopolymerization opens new doors towards nanophotolithography using visible light sources, without being limited by the diffraction limit. Many efforts have been dedicated during recent years to propose innovative methods to push the limits and constraints of nanofabrication processes [43]. Among them, some processes take advantage of the possibility to perform far-field imaging beyond the diffraction limit [44–47].

Photochemical reactions can be confined at the nanoscale by controlling the diffusion rates of reactive species. Near-field photopolymerization appears in this context as an alternative approach for reducing the size of features and/or fabricating sophisticated hybrid nanostructures.

2.2. Photopolymerization

The two main routes for photopolymerization are cationic and free-radical processes, depending on the nature of the reactive species involved in the polymer chain growth.

Cationic photopolymerization in the context of micro-nanopatterning usually includes an epoxy-based monomer. The epoxy group can be opened in acidic conditions, leading to the polymerization of epoxy monomers. The photoinitiator for such polymerization is a photoacid generator species. SU8, a commercially available cationic negative tone photoresist [48], was used in the framework of plasmon-induced nanostructuring in several examples. Among the first examples, Srituravanich *et al* produced sub-wavelength dots using aluminum hole arrays as a plasmonic photomask [49]. Structures as small as 90 nm with a period of 170 nm could be generated using 365 nm irradiation. Silver 2D hole array masks were also used to generate 60 nm half-pitch resolution dots using SU8 [50].

2.3. One-photon versus two-photon photopolymerization

Nonlinear processes are frequently desired for nanofabrication approaches since the incident light profile usually does not have a sharp spatial distribution. The response function of the material is, therefore, used to sharpen the object produced by lithographic process. Several chemical or physical principles can be involved. Two-photon absorption is a way to generate highly nonlinear responses. Using this principle, Sundaramurthy *et al* achieved the polymerization of SU8 photoresist under femtosecond laser irradiation [51]. The multiphoton absorption regime is reached when a high density of photons (either temporally or spatially) interacts with an organic molecule. These specific conditions are usually obtained using a femtosecond pulsed laser and lenses with high numerical apertures. The enhancement of the electromagnetic field due to the plasmon resonance is enough in some configurations to obtain multiphoton absorption with incoherent light. Ueno *et al* demonstrated that photopolymerization of SU8 can be triggered by a halogen lamp emitting in the W cm^{-2} range (600–900 nm) (figure 4). The authors stressed that in the nanogap between metal nanoparticles, the enhancement factor is strong enough to reach

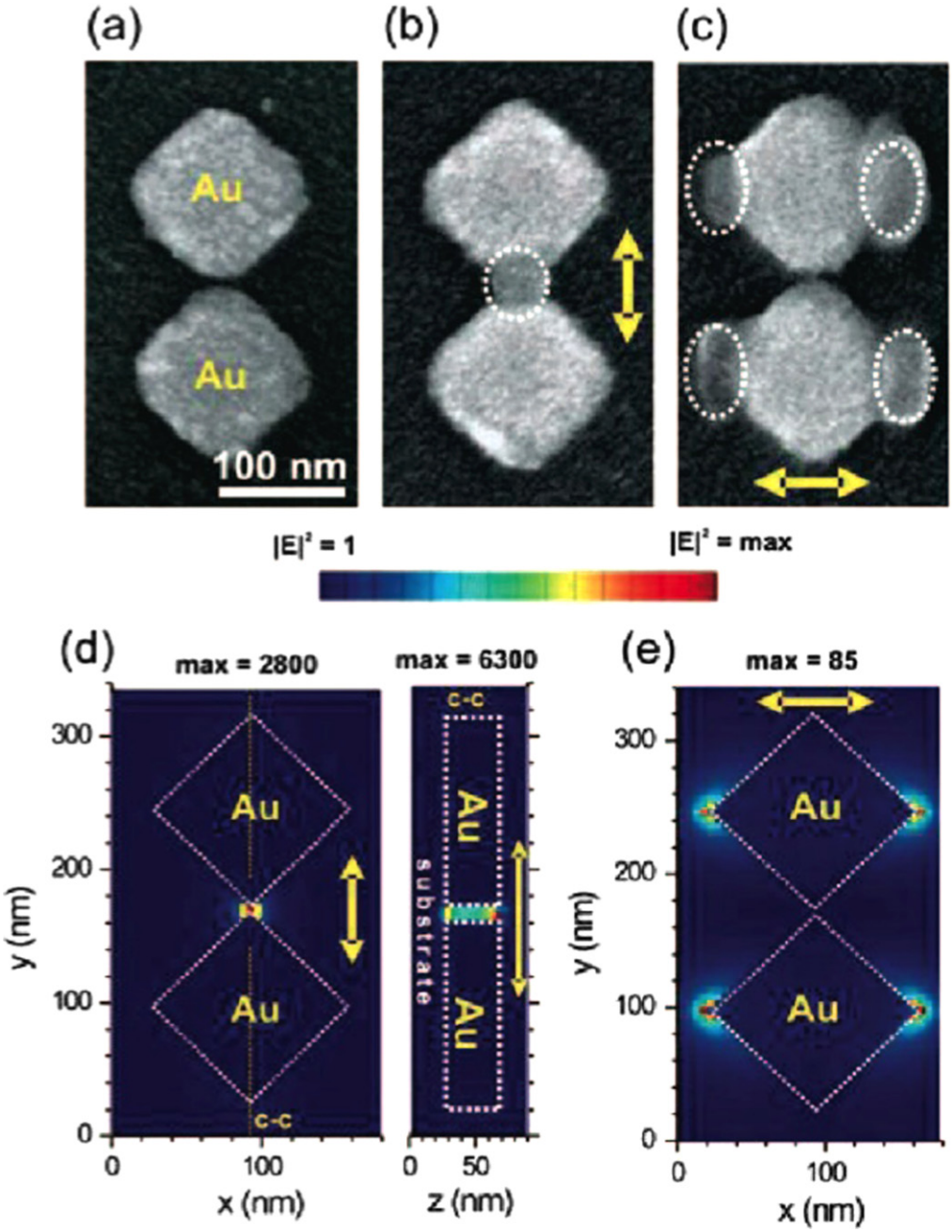

Figure 4. (Top) SEM images of photopolymerized regions on gold nanoblock dimers for two polarization states. (Bottom) Theoretical results of the distribution of the electromagnetic field around the nanogap showing the good agreement with polymerization. Reprinted with permission from [52]. Copyright 2008 American Chemical Society.

regimes for which two-photon absorption and subsequent polymerization is possible [52].

3. Our approach: plasmon based free-radical photopolymerization

Over the past decade, we have been developing an approach of plasmon-assisted free-radical photopolymerization. The advantage of this reaction is to offer a wider range of photoinitiators, especially in the visible range, able to trigger the photopolymerization reaction. Thus, it is possible to finely adjust the wavelength sensitivity of the photopolymer with the resonance of metal nanoparticles. Additionally, we will see that it is possible to functionalize the material to make it active.

The principle of our approach is illustrated in figure 5 [53]. The photopolymerizable formulation (PPF) is made up of three basic components: a sensitizer dye, a co-synergist amine, and a multifunctional acrylate monomer, pentaerythritol triacrylate (PETIA). PETIA is used as received from the supplier and forms the backbone of the polymer network. The co-synergist amine is the methyldiethanolamine (MDEA). For example, the Eosin-Y (2′,4′,5′,7′-

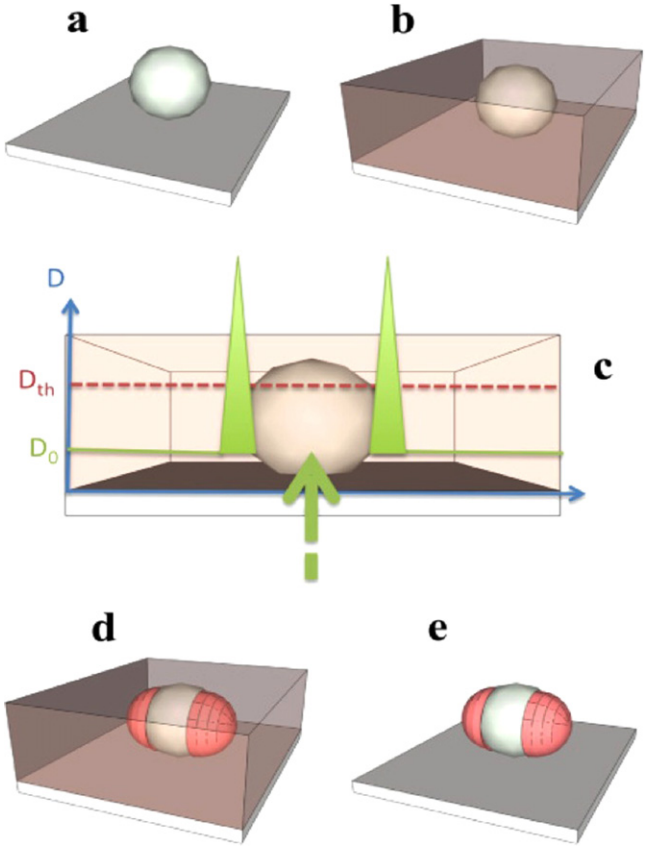

Figure 5. Scheme of the approach. (a) Metal NP deposited on a functionalized glass substrate. (b) Deposition of the photopolymerizable formulation. (c) and (d) Plasmon based near-field photopolymerization of PPF leading to polymer nanostructures corresponding to the LSP intensity distribution. (e) The resulting hybrid nanoparticle is revealed by rinsing procedure. Reprinted with permission from [53]. Copyright 2010 American Chemical Society.

tetrabromofluorescein disodium salt) can be used as the sensitizer dye that makes the system sensitive to the spectral region from 450 nm to 550 nm. As another example, methylene blue (MB) molecules make the formulation red-sensitive. This liquid system is very flexible as it is possible to modify the components independently to adjust the physical and the chemical properties of the formulation, namely, viscosity, spectral sensitivity, and polymerization threshold energy. A typical mixture contains 0.5 wt% of Eosin-Y and 4 wt% of MDEA. After optical absorption from the excited LSP, the Eosin-Y is excited to its single state, followed by non-radiative intersystem crossing to create a triple state. The excited molecule interacts through electron and proton transfer with the amine to create radicals that interact with the monomer, and trigger the polymerization. An important parameter that characterizes this formulation is the threshold dose of energy, D_{th}, generally expressed in mJ cm^{-2}. This parameter is the minimum dose of photonic energy that should be provided to the system to start the polymerization. Below D_{th}, the energy is lost through a couple of reactions including formation of peroxides from radicals. We will show that our method relies on this parameter.

Metal nanoparticles on a substrate (figure 5(a)) are homogeneously covered by a synthesized free radical PPF possessing high-resolution visible-light sensitivity (figure 5(b)).

The polymerization is activated by laser irradiation (plane wave of controlled polarization state) with wavelengths overlapping with both the PPF absorption spectrum and the NPs plasmon resonance. The exposure dose (D_0) is chosen to be weaker than D_{th}, the threshold dose necessary for reticulation (figure 5(c)). Therefore, photopolymerization is not expected to occur in the absence of NPs: because of the field enhancement at the plasmon resonance (figure 5(c)), the effective dose near the metallic nanoparticles can get higher than the threshold D_{th} to initiate the chain reaction leading to local polymerization (figure 5(d)). After irradiation, any monomer that is not reticulated is removed by a rinsing procedure (figure 5(e)) and the resulting hybrid nanostructure is characterized by an atomic force microscope (AFM) and optical spectroscopy. The size of the polymer wings attached to NPs is related to the strength and the depth of the plasmonic optical near-field.

4. Achievement and applications

4.1. Studying and quantifying plasmonic near-fields

The method constitutes an efficient way of probing the intensity of the optical near-field. It can be viewed as a near-field photographic approach where the 'pictures' are read by AFM, ruling out any diffraction-limited far field effects. This idea was first introduced in [53].

By analyzing precisely the dimension of the polymerized regions as a function of the relevant parameters (incident energy, local position, direction of polarization, etc), it is possible to get valuable quantitative information about the plasmonic near-field intensity. It would be very difficult to acquire such information by using alternative methods like scanning near-field optical microscopy [54], photo emission electron microscopy [55], or electron energy loss spectroscopy [56].

Two illustrating examples are shown in figures 6 and 7. The first example concerns gold nanocubes [57]. The optical properties of metal nanocubes have been the focus of recent experimental and theoretical works (e.g. see [58–60]). Most of these works have focused on the unique properties of the cubes, especially enhanced local electromagnetic fields, particularly at the eight vertices and along the twelve edges of the cube, when illuminated with light. To date, only little is known about the local near-field optical properties of metal nanocubes, since most of the plasmonic studies were carried out in the far-field. However, to pave the way for tailoring nanostructured electromagnetic fields using nanocubes, a detailed characterization of their near-field properties is essential. Our method relying on nanoscale photopolymerization allows one to address this challenge. Figure 6(A) shows a scanning electron micrograph (SEM) of a single, 60 nm edge, gold nanocube. It presents a dipolar

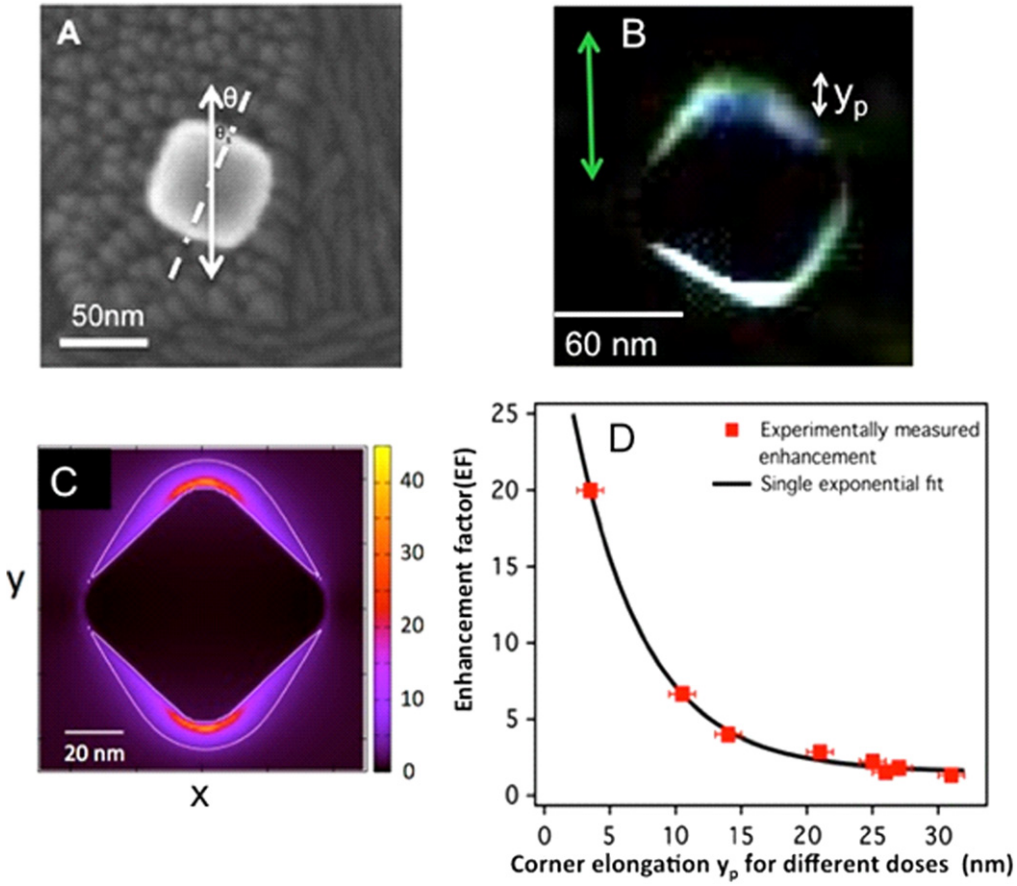

Figure 6. Investigation of the near-field plasmonic intensity at the surface of a gold nanocube. (A) SEM image of one single nanocube. θ is the cube orientation. The arrow represents the direction of the incident polarization used for photopolymerization. (B) Differential AFM image of the hybrid nanosystem obtained by plasmonic near-field photopolymerization. (C) Calculated near-field intensity enhancements $|E|^2/|E_0|^2$ in an $n=1.5$ medium. Light is incident from below along the z-axis and is polarized along the y-axis. The observation plane is at $z=6$ nm below the top of each cube. The contour lines correspond to $|E|^2/|E_0|^2 = 40$, illustrating the threshold to be exceeded for $D_0 = 0.025 \times D_{th}$. (D) Demonstrated intensity enhancement factor as a function of the measured polymer extension along the cube corner. The black curve is an analytical fit. Adapted with permission from [57]. Copyright 2012 American Chemical Society.

plasmon resonance in the 500–600 nm spectral range, corresponding to the spectral sensitivity of the PPF used. The polarization used for photopolymerization is vertical and the orientation of the cube side edge relative to this polarization is described by the angle θ. The experiment was performed with $\theta = 45°$, i.e. with the cube corner parallel to the polarization. In this situation, the local field enhancement factor is expected to be significant due to the lighting rod effect.

An AFM image of the hybrid 'nanocube + polymer' system is acquired, from which a background AFM image of the nanoparticle preceding the photoexcitation has been subtracted, leading to a differential AFM image that highlights the integrated polymer nanostructures, regardless of the initial topography, as a signature of the local light. A representative differential AFM image can be seen in figure 6(B). In particular, polymer elongation is seen along the polarization direction, while no polymerization is induced where the unit surface normal vector is perpendicular to the laser polarization direction. Figure 6(B) was obtained with an incident dose of 25% of D_{th}. It is worth comparing this figure with the expected calculated near-field intensity (figure 6(C)) where the iso-intensity contour line represents the threshold to be exceeded for polymerization. From figures 6(B) and (C), it turns out that the polymerization occurred inside the zone defined by the iso-intensity contour, while the energy outside was not high enough to trigger the polymerization. Based on the knowledge of the polymer extending along the corner (y_p in figure 6(B)), it has been possible to quantify valuable features related to the nanocube plasmonic field. This quantification is made in the following way. Let us consider that the near-field of the excited nanocube is characterized by an exponential decay. Along the y-axis, the local dose D at the cube corner can be expressed as

$$D = F_{max} D_0 \exp(-\alpha y), \quad (1)$$

where F_{max} is the maximum (at the surface) intensity enhancement factor related to the LSP resonance, α is the spatial decay rate of the field intensity (α^{-1} is its characteristic decay length), and y is the distance from the surface of the metal nanoparticle in the y-direction.

We have already established that photopolymerization only occurs when $D > D_{th}$. By applying this condition to

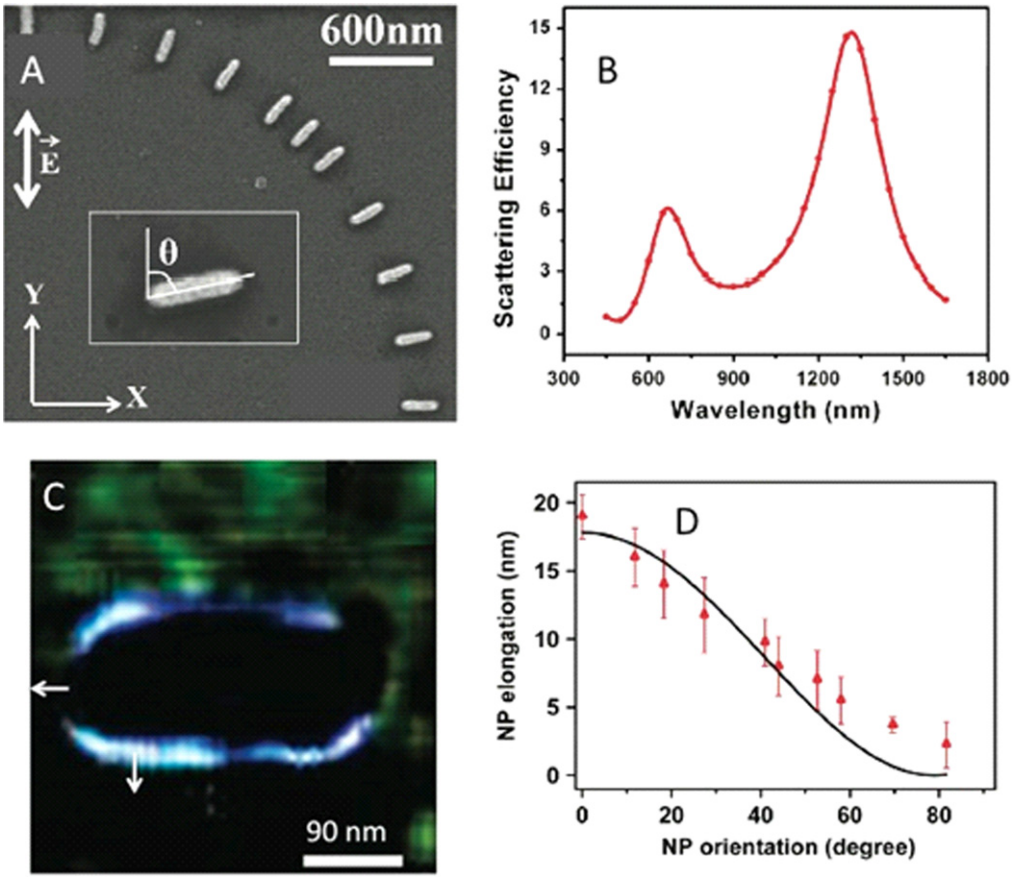

Figure 7. Mapping non-resonant electromagnetic effects. (A) Representative SEM showing eleven differently oriented GNRs. The incident field polarization direction is represented by the double white arrow. The inset of (A) shows the angle θ between the nanorod major axis and the polarization direction. (B) Calculated far-field scattering spectrum for a single rod, embedded in a medium of refractive index 1.485, corresponding to that of the photopolymerizable solution, illustrating the localized surface plasmon response of both nanorod axes. (C) Differential AFM image of the hybrid structure resulting from a plasmonic phopolymerization with $\theta = 90°$. The white arrows represent the surface normal unit vector at two locations. (D) Polymer elongation at the rod extremity (along the long axis) as a function of θ. Red dots: experimental data. Black curve: analytical model (see text). Adapted with permission from [62]. Copyright 2011 American Chemical Society.

equation (1), one can obtain

$$\exp(-\alpha y) \geqslant \frac{D_{\text{th}}}{F_{\max} \times D_0}. \tag{2}$$

By simplifying equation (2), one can get the maximum distance $y_{\max}$ away from the Au nanocube at which the effective dose overcomes D_{th} as

$$y_{\max} = \alpha^{-1} \ln\left(F_{\max} \times \frac{D_0}{D_{\text{th}}}\right). \tag{3}$$

Equation (3) can be rewritten as

$$y_{\max} = \alpha^{-1} \ln\left(F_{\max} \times f\right), \tag{4}$$

where f (in %) represents the incident dose, normalized by the threshold.

$y_{\max}$ is equal to y_{p} that is experimentally measured. For example, an elongation of $y_{\text{p}} = 3.5$ nm was measured for an incident dose of $f = 5\%$, which implies that an enhancement factor of at least 20 (=1/f) is expected at the corner of the nanocube at the y_{p} distance. This (3.5 nm; 20) plot is represented in figure 6(D). In order to accurately determine $F_{\max}$ and α, many exposures of different doses were performed on numerous identical nanocubes, resulting in figure 6(D) that shows the values of 1/f, deduced from $1/f = D_{\text{th}}/D_0$, as a function of the polymer elongation $y_{\text{p}} = y_{\max}$. The data follow a single exponential decay reflecting the near-exponential decay of the plasmon near-field. 1/f can be deduced from equation (4) as $\frac{1}{f} = F_{\max}\, \text{e}^{-\alpha y_{\max}}$. Thus, when fitting the experimental data with an exponential function, one can deduce the values of the fitting parameters $F_{\max}$ and α^{-1} as 35 and 5 nm, respectively. This simple example illustrated well the high capability of the method for quantitative near-field analysis. The analysis of the influence of θ was performed as well, allowing one to discuss the importance of incident field excitation in such structures [57]. This point will be discussed in the text relevant to figure 7.

The second example deals with non-resonant metal nanosystems. While resonant surface plasmons have been widely studied over the past 20 years, only few experimental studies on non-resonant effects have been reported (e.g. [61]) because off-resonant excitations generate weak and very localized fields that are extremely difficult to measure. In that

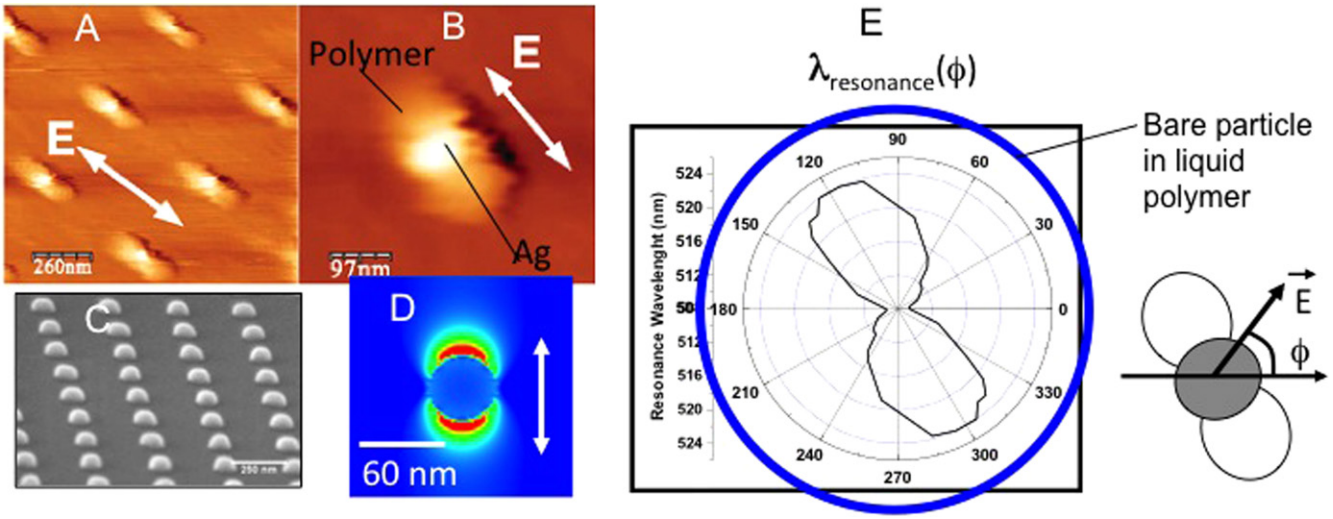

Figure 8. Structuring the surrounding environment by plasmonic photopolymerization (A) and (B) AFM image taken after procedure applied to silver hemispherical nanoparticles. (C) SEM image of the nanoparticles before exposure. (D) Calculated intensity distribution during the photopolymerization ($\gamma = 514$ nm). (E) Polar diagram showing the position of the plasmon resonance peak of the hybrid particle as a function of the direction of incident field. The blue circle illustrates what would be obtained in an anisotropic polymeric material. Reprinted with permission from [63]. Copyright 2007 by the American Physical Society.

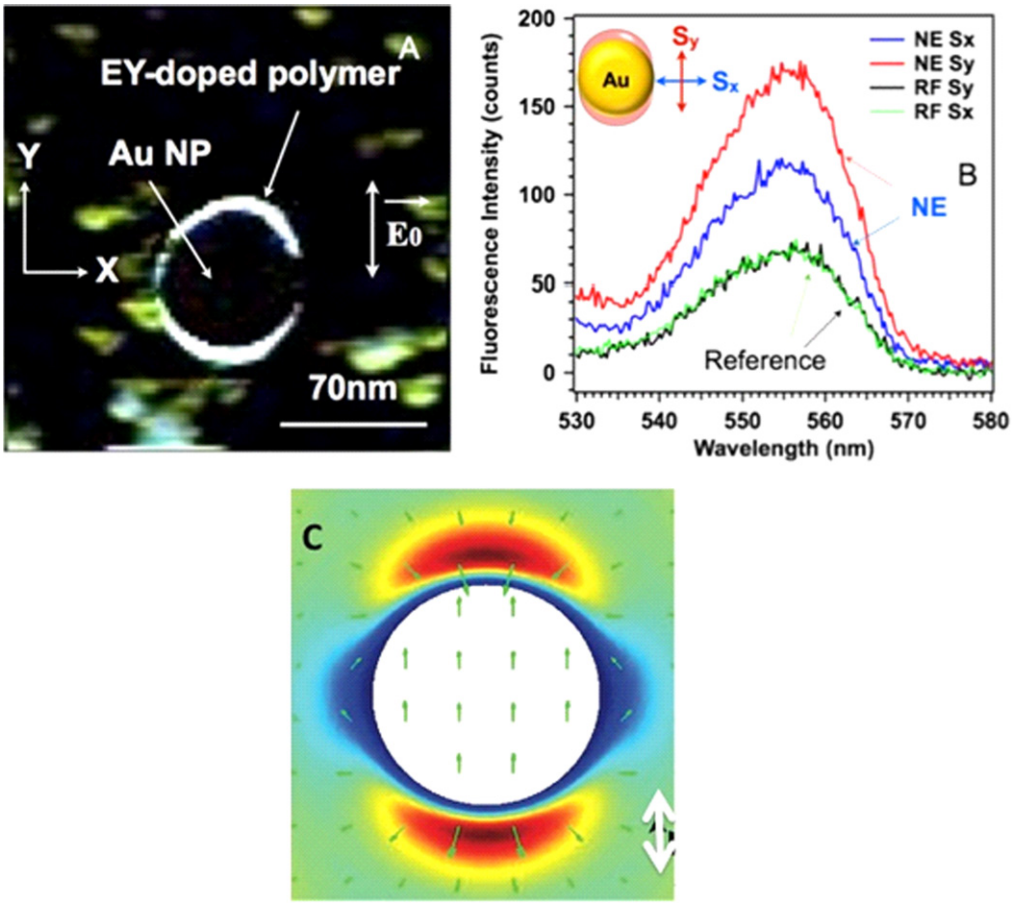

Figure 9. (A) Differential AFM image showing the topography of a hybrid nano-emitter based on a gold nanosphere of 70 nm diameter. The highlighted nanostructures represent the integrated photopolymer structures with a thickness of 15 nm each. (B) Polarization-dependent fluorescence signal ($\lambda_{ex} = 514$ nm) of the nano-emitter with intensity higher when the incident light is polarized along *Y*-axis than along the *X*-axis. References were collected from 2 μm away from the NE with an incident field along *X* (in green) and *Y* (in black) axes. (C) Top view of the emission rate map. The calculation was done in a polymer of $n = 1.48$. Reprinted with permission from [66]. Copyright 2014 AIP Publishing LLC.

case, the oscillating charges vibrate in phase and the quasi-electrostatic case can be considered. The approach of plasmonic photopolymerization has been applied to non-resonant metal nanosystems [62]. The sample used is shown in figures 7(A) and (B). It consists of gold nanorods (GNRs) having a different orientation θ relative to a fixed linear polarization along the *y*-axis. As shown in figure 7(B), within the PPF, such nanorods present two dipolar resonant modes at 680 nm (transverse mode) and 1350 nm (longitudinal mode). We used a wavelength of 530 nm for triggering the polymerization, which is pretty far from the resonant plasmonic modes. Figure 7(C) is the resulting AFM differential image in the $\theta = 90°$ case. Here, the exposure dose was chosen to be 65% of the threshold dose, still lower than the threshold but high enough to be sensitive to the weak, off-resonance intensity enhancement. The polymer spatial extension turns out to be maximum when the unit vector normal, **n**, to the rod surface is aligned with the polarization direction. Conversely, the polymer extension is null when the unit vector is perpendicular to the polarization, as one can see at the GNR extremity in figure 7(C). This effect can be interpreted in terms of polarization surface charge density. Let us consider the free electrons at the metal surface (belonging to the metal itself) that are driven by the incident field and that re-radiate light, resulting in a localized optical near-field. This excitation is quantified by the dielectric susceptibility of the metal. We propose that the local polymerization is driven by these excited surface charges that are related to the electric field discontinuity at the rod interface, following the usual boundary condition

$$E_{1n} - E_{2n} = \left(\rho_{s,pol}/\varepsilon_0\right) = \chi \mathbf{n} \cdot \boldsymbol{E_o}, \tag{5}$$

where E_{1n} and E_{2n} are the normal components of the electric field inside and outside of the rod, respectively, $\mathbf{E}_0$ is the incident electric field vector, $\rho_{s,pol}$ is the surface density of polarization charges, and χ is the metal electric susceptibility. In turn, the excited surface charges create their own electric field that is responsible for a weak field enhancement on the rod surface, and hence subsequent polymerization.

The polymer spatial extension was measured at the extremities of the rod as a function of θ (see figure 7(D)). A clear polarization sensitivity is demonstrated, as the expression of the scalar product in equation (5). It can be compared to a fit extracted from an analytical model (black full line) that is based on simple considerations summarized as follows. We consider that the electric field at the GNR surface results from a coherent constructive interference (in the off-resonant case, photoinduced charges vibrate in phase with the incident field) between the incident field and the local field re-radiated by the induced polarization vibrating charges, via the local susceptibility. The spatial polymer extent is assumed to be proportional to the resulting intensity. Appropriate fitting parameters allowed us to get a realistic value of the local effective surface susceptibility [62].

4.2. Hybrid nanostructures presenting new optical properties

Besides the possibility of quantifying the plasmonic near-field, the approach turned out to allow for photoinduced synthesis of new hybrid nanosystems having unique optical properties. A first example is shown in figure 8 [63]. It concerns a passive structure in the sense that no optical activity in terms of light emission from the polymer is considered for the moment. Figures 8(A) and (B) show the result of the plasmon-based photopolymerization on silver hemispherical nanoparticles produced by e-beam lithography (figure 8(C)). Two symmetric polymer lobes adjacent to the particles can be observed, resulting in metal–polymer hybrid particles. The two lobes originate from the excitation of a particle dipolar surface plasmon resonance, as numerically illustrated in figure 8(D) obtained through a finite difference time domain calculation. The field distribution associated with the resonance is enhanced in a two-lobes region oriented along the incident polarization. The localized nanoscale photopolymerization is the result of the inhomogeneous field distribution. The two lobes can thus be viewed as a three-dimensional polymer molding of the locally enhanced optical fields.

Figure 8(E) is a polar diagram of the surface plasmon resonance peak of the obtained hybrid nanostructure. We measured fifty spectra of the hybrid particles for different angles of polarization, as illustrated at the right side of figure 8(E). The two polymerized lobes clearly induced a quasi-continuously tunable LSP resonance in the 508–522 nm range. The local polymerization turns out to lead to two new plasmon eigenmodes centered at 508 and 522 nm, respectively. For any polarization angle, a linear combination of the two eigenmodes is excited, with respective weights depending on the polarization direction. We conclude that the apparent continuous plasmon tuning is the result of the spectral linear combination. The anisotropic behavior can be compared to what would be observed in the case of a bare particle embedded in the isotropic liquid polymer (see blue circle on figure 8(E)). Before local photopolymerization, metallic nanoparticles are characterized by a $C_{\infty v}$ symmetry corresponding to rotation around the C_v axis. After polymerization, the two polymerized lobes induce a new lower symmetry: C_{2v}, for which any pattern is reproduced by a π in-plane rotation. This new symmetry induces the breakdown of the LSP spectral degeneracy. We can also consider that a nanoscale artificial ellipsoid of indexes was integrated in the vicinity of the silver particle, making it polarization sensitive. Additionally, it was possible to get a polar distribution of the effective refractive index from figure 8(E), simply by expressing the index shift as a function of the wavelength shift in the expression of the polarizability of the particle seen as a plasmonic nanosensor [63].

Figure 8 illustrates in a remarkable way the possibility to control and structure the spatial environment of metal nanoparticles, resulting in new and unique optical properties.

4.3. Advanced active hybrid nanostructures for nanophotonics

As an indispensable component of PPF, dye molecules located within the near-field of metal nanoparticles can be trapped by the integrated photopolymers. Thanks to the anisotropic distribution of dipolar mode plasmons supported by metal nanoparticles, the obtained metal/polymer nanostructure is thus a plasmonic nano-emitter (NE), whose dye molecules are anisotropically spatially distributed. Unlike conventional hybrid plasmonic light-emitting systems with a random or isotropic distribution of dye molecules around the metal nanoparticle [64, 65], this anisotropic spatial distribution of dye allows an optical selection of the molecules by using incident polarization. A recent study has been published on an anisotropic NE based on an isolated gold nanosphere with a diameter of 70 nm [66]. Linear polarization of the incident light produced 15 nm thick polymer structures integrated in the *Y*-axis as figure 9(A) presents. This NE was characterized optically by fluorescence from Eosin-Y molecules excited by a 514 nm laser with a polarization switchable between *X*- and *Y*-axes.

It was found that the NE was more efficiently activated when the excitation light was polarized along *Y*-axis than along the *X*-axis (figure 9(B)). This optical anisotropy resulted from the overlap between the dipolar plasmonic mode and the active medium, both of which presented anisotropic spatial distributions. When polarized along the *Y*-axis, the excitation light led to a plasmonic field oriented in *Y*, which completely overlapped with the dye-containing active medium. In comparison, the plasmonic field was perpendicular to the distribution of the active medium of the NE under the incident polarization along the *X*-axis. The different spatial overlap caused a different number of molecules to be excited by the near-field. Background-corrected fluorescence from a single NE presented 2.2-times higher intensity with a polarization parallel (S_y) to the active medium distribution than perpendicular (S_x) to it.

The emission rates of a dye molecule in free space γ_{em}^0 and in the close vicinity of a metal nanoparticle γ_{em} are well known as

$$\gamma_{em}^0 = q\,\gamma_{ex}^0 \tag{6}$$

and

$$\gamma_{em} = Q\,\gamma_{ex} \tag{7}$$

respectively, where q is the intrinsic (free space) quantum yield and γ_{ex}^0 is the excitation rate of the dye molecule in free space, Q is the nanoparticle-modified quantum yield and γ_{ex} is the excitation rate of the dye molecule by the local electric field. Q can be calculated from the Mie Theory [66, 67]. γ_{ex}^0 and γ_{ex} are expressed as functions of the incident field and local electric field, i.e., $\gamma_{ex}^0 \propto |\boldsymbol{E}_0 \cdot \boldsymbol{p}|^2$ and $\gamma_{ex} \propto |\boldsymbol{E}_{loc} \cdot \boldsymbol{p}|^2$, respectively, where $\boldsymbol{p}$ is the molecular transition dipole moment and E_{loc} is the local near-field. It should be stressed out that the molecular dipole orientation was not controlled in this experiment. An averaged molecule orientation was therefore applied for the calculation [66, 67]. As a consequence

$$\frac{\gamma_{em}}{\gamma_{em}^0} = \frac{Q}{q}\left|\frac{E_{loc}}{E_0}\right|^2. \tag{8}$$

The calculated spatial distribution of free-space-normalized emission rate of Eosin-Y molecule in the vicinity of a gold nanosphere is shown in figure 9(C). This normalized emission map shows a maximum normalized emission of $\gamma_{em}/\gamma_{em}^0 = 1.45$.

To some extent, figure 9(C) represents the probability of emission of the dipole emitter as a function of its position in the vicinity of a gold nanoparticle that is illuminated with a field parallel to the *Y* axis. For example, the dark ring in the close vicinity of the particle tells us that the dipole can not emit light due to the quenching effect associated to a non-radiative energy transfer. In the anisotropic hybrid NE, two key factors have actually to be considered. One is the probability of the presence of dye molecule in the plasmonic near-field. The other is the probability of light emission of these molecules. The latter has been expressed in equation (7) and has been calculated in figure 9(C). This is a factor to be considered in all plasmon-modified fluorescence studies regardless of the NE configuration. The probability of spatial presence of molecules, however, is what we control via nano-photopolymerization. Figure 9(A) can be viewed as a map of probability of presence of dipole emitter trapped in the polymer.

It modifies equations (6)–(8) to

$$\gamma^0{}_{em} = \phi_{out}\, q\, \gamma^0{}_{ex}, \tag{9}$$

$$\gamma_{em} = \phi_{in}\, Q\, \gamma_{ex}, \tag{10}$$

$$\left(\frac{\gamma_{em}}{\gamma_{em}^0}\right)_{NE} = \frac{\phi_{in}}{\phi_{out}}\frac{Q}{q}\left|\frac{E_{loc}}{E_0}\right|^2, \tag{11}$$

where ϕ_{in} is the probability of the presence of molecule inside the photopolymer nanostructure, while ϕ_{out} is the probability of the presence of molecule outside the photopolymer nanostructure. After photopolymerization and rinsing, molecules that are not trapped in the photopolymer nanostructures are expected to be removed by solvent. In other words, the probabilities of molecular presence outside and inside the photopolymer nanostructures are expected to be 0 and 1, respectively. In reality, however, as figure 9(B) illustrates, the rinsing process is not perfect, which led to the detection of a reference signal of fluorescence signal 2 μm away from the hybrid NE. The spectra in black and green were collected with polarizations along the *Y*- and *X*-axes, respectively. Obviously the reference signals were not polarization sensitive. The probability of the molecule presence falls in the band of $0 < \phi_{out} < 1$ instead to equal 0. Consider the situations of NES_y and RF curves in figure 9(B) that satisfies equations (10) and (9), respectively, we obtain $(\gamma_{em}/\gamma_{em}^0)_y = \mathrm{NE}S_y/\mathrm{RF} = 2.5$ from equation (11). ϕ_{out} can be deduced from the ratio of equation (11) over equation (8): $\phi_{in}/\phi_{out} = 2.5/1.45$. Inside the photopolymer, when we set $\phi_{in} = 1$, $\phi_{out} = 0.58$ can be obtained.

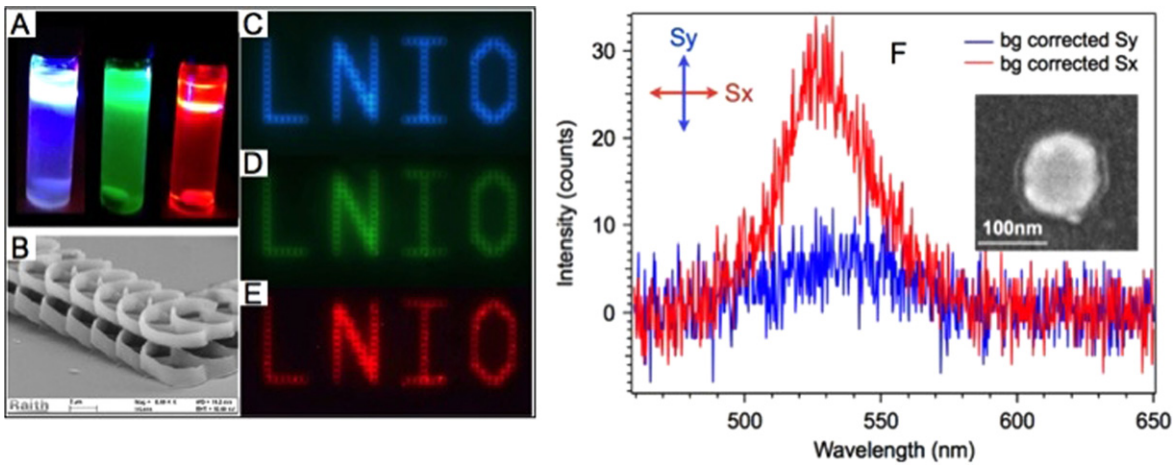

Figure 10. (A) Photopolymerizable solutions doped with different QDs that emit at 460 nm, 510 nm, and 620 nm (from left to right), respectively. (B) SEM image of photopolymer structures fabricated by laser scanning photo-lithography with the QD-containing polymerizable solutions. Fluorescence images of patterns of photopolymer structures doped by QDs emitting at (C) 460 nm (D) 510 nm and (E) 620 nm. (F) Background-corrected fluorescence spectra (two perpendicular incident polarization) from the green QDs that are embedded in the polymer lobes of a hybrid nano-emitter produced by two-photon plasmonic nano polymerization. The inset shows a SEM image representing the hybrid nano-emitter with polymer lobes oriented in the *X*-axis.

In the case of NES_x, considering equation (5), the optical near-field enhances the local electromagnetic field at any point in the vicinity of metal nanoparticle except for the points where $\mathbf{n} \perp \mathbf{E}_{\mathrm{loc}}$. As a consequence, fluorescence of a certain percentage (η) of the molecules in the photopolymer nanostructure can be enhanced by the near-field when the incident polarization is oriented perpendicular to the polymer lobes [66]. In this situation, equation (11) can be modified as

$$\left(\frac{\gamma_{\mathrm{em}}}{\gamma_{\mathrm{em}}^{0}}\right)_{x} = \eta\frac{\phi_{\mathrm{in}}}{\phi_{\mathrm{out}}}\frac{Q}{q}\left|\frac{E_{\mathrm{loc}}}{E_0}\right|^2 + (1-\eta)\frac{Q}{q}\left|\frac{E_{\mathrm{loc}}}{E_0}\right|^2. \quad (12)$$

The first component on the right side of equation (12) represents the molecules excited by both S_x and S_y configurations, while the second component represents the molecules distributed in the near-field of S_x and outside the near-field of S_y. From figure 9(B) one sees $(\gamma_{\mathrm{em}}/\gamma_{\mathrm{em}}^{0})_x = \mathrm{NE}S_x/\mathrm{RF} = 1.69$. The value of $\eta = 0.33$ can be consequently deduced from equation (12). In other words, one third of the dye molecules in the photopolymer can be excited by the plasmonic field under both polarizations.

As a conclusion, the effective emission from the anisotropic NE depends on the spatial overlap between the probability of emission and the probability of presence of dipole emitters. In other words the product of these two probabilities gives us an idea of the effective light emission.

Despite the observation of anisotropic fluorescence resulting from the dye-doped photopolymer spatial distribution and its overlap with the excitation near-field, there is no doubt that this hybrid nanostructure has to be improved in order to amplify the optical anisotropy. For a certain probability of the molecules outside the photopolymer nanostructures, our attention turns to the quantum emitter around the nanoparticles. Quantum yield is an element that can be improved. Additionally, the dye molecules in this study have participated in the photopolymerization process, which resulted in the photo-bleaching of most of the molecules [68]. It is thus reasonable to think about another candidate for emission: QDs.

With QDs grafted by covalent bonds on the PETIA molecules, this type of polymerizable solution allows us to trap QDs in the integrated photopolymer structures. Figure 10(A) shows a photo of photopolymerizable solution doped with three different QDs, ZnCdS/ZnS emitting at 460 nm, CdSe/ZnSeS emitting at 510 nm, and CdSe/CdS/ZnS emitting at 620 nm, respectively. Figure 10(B) is the SEM image of a high resolution far-field laser scanning lithography with the QD-containing photopolymerizable systems. Figure 10(B) was obtained via two-photon absorption photopolymerization.

Fluorescence images of the three different types of QD-doped photopolymer structures are shown in figures 10(C), (D) and (E), respectively.

On a 100 nm diameter gold nanodisk, two-lobe photopolymer nanostructures were integrated via two-photon polymerization to trap QDs that emit at 510 nm in the active medium in the near-field of the nanoparticle. Figure 10(F) illustrates the resulting background corrected fluorescence spectra under incident polarizations along (S_x) and perpendicular (S_y) to the polymer nanostructures. As is shown in the SEM image (inset of figure 10(F)), photopolymer nanostructures were oriented along the *X*-axis. The polarization-dependent fluorescence indicates a 6-times higher intensity of S_x than S_y, which is due to the spatial overlap of the QD-doped active medium and the plasmonic near-field of the gold nanodisk. The optical anisotropy of the NE has been considerably enhanced by substituting organic dye to QDs.

Another example is to position dye molecules in the gap of nanodimers via the photopolymerization process. It should be stressed that other than fluorescence spectroscopy, surface-enhanced Raman scattering (SERS) can be used as well to probe the presence of molecules at the plasmonic hot spots.

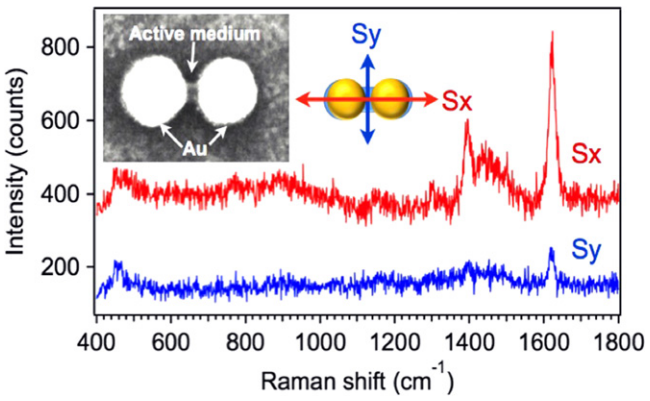

Figure 11. Polarization-dependent SERS signals from MB molecules. Inset SEM image shows the topography of the hybrid nanodimer with MB-doped photopolymer integrated in the gap.

The MB molecule is known as a good SERS probe and was thus applied in this study. With incident light polarized along the interparticle axis of the nanodimer, MB molecules can be selectively positioned in the active medium formed in the nanodimer gap. MB molecules were initially embedded in the PPF to make it sensitive to the red light that corresponds to the wavelength of LSP resonance of the dimer. Figure 11 presents the polarization sensitivity of the SERS signal on a single gold nanodimer/photopolymer hybrid nanostructure with initial gap size of 10 nm. The inset shows a topographic SEM image that presents different contrasts on metal and photopolymer. As the spectra indicates, the characteristic SERS mode at 1620 cm^{-1} is assigned to the stretching (C=C) ring of MB molecule. The SERS signal obtained with an incident polarization along the gap (S_x) is approximately 5 times higher than that perpendicular to the gap (S_y).

As for figure 10, this polarization sensitivity observed in figure 11 is believed to result from a tunable spatial overlap between the plasmonic near-field and active molecules.

4.4. Application to nanophotochemistry

The studies carried out have revealed some very specific aspects regarding free-radical photopolymerization and associated chemistry that are worth being detailed. Using the plasmon-assisted configuration for local irradiation appears as a very interesting configuration for investigating nanophotopolymerization. It is important to examine in detail the molecular pathway leading to photopolymerization (figure 12). The absorption of a photon leads to the excited singlet state of the Eosin-Y, and then to its triplet state by intersystem crossing. From the triplet state, the dye can react with the amine to produce the first radical able to induce the free-radical polymerization of the methacrylate monomer. A trifunctional monomer is used so a rapid crosslinking of the polymer network is usually observed [69]. The right part of the scheme describes the inhibition processes that are due to the oxygen dissolved in the photopolymer. Oxygen can react with the triplet state of the dye, or with radicals, to create peroxide radicals that are not active for polymerization [70]. Usually, in free-radical polymerization, these later processes are considered to be detrimental because less reactive species are available for polymerization. In micro and nanofabrication, such a molecular phenomenon is advantageously used to ensure a precise control of the polymerization volume. However, the presence of oxygen considerably affects the kinetics of photopolymerization and needs to be taken into account.

One major effect is on the threshold of polymerization, which depends on many chemical, physico-chemical, and photonic parameters [72]. From the triplet state, a protonated Eosin radical can be formed by reaction on MDEA. This radical is known to be ineffective for initiating polymerization. However, several reactions of this radical have to be considered [73]. First, it can react with another protonated Eosin radical to regenerate an Eosin molecule in the leuco form. The later form does not absorb at 532 nm, and the consequence of this reaction is the progressive bleaching of the Eosin formulation. Second, the protonated Eosin radical can undergo a disproportion reaction with other radicals (deprotonated amine radical, peroxide radicals or free-radicals of the growing polymer chains), where in this case, the Eosin is regenerated to its fundamental state. Such processes regenerate the Eosin in an active state that can photosensitize again other MDEA reactions.

By measuring the lateral extent of the lobes deduced from differential images (such as shown in figure 9(A)), we investigated the role of irradiation dose on the polymerization at the nanoscale. Interestingly, it was demonstrated that the exposure time and the irradiation power are not equivalent to each other in terms of the spatial extent of the polymerization, although they correspond to the same energy (figure 13). For a given dose, the lateral extent of polymerization is more pronounced for lower intensity, which is different from previous studies of microscale photofabrication [72].

The behavior observed at the microscale [72] was interpreted as follows. The inhibition role of oxygen is more pronounced at low intensity (i.e. long irradiation times) because the consumption of oxygen is slow enough to allow for a continual replenishment from the surroundings. The polymerization process starts only when the oxygen concentration in the photopolymer droplet is low enough, which implies that replenishment increases the inhibition time. For higher incident power, the inhibition is less sensitive because oxygen diffusion has no time to proceed efficiently relative to the rate of new photons injected into the system. What we observed at the nanoscale reveals an opposite behavior to what was seen at the microscale.

Taking into account that the typical dye concentration is 0.5 wt%, and assuming a homogeneous distribution of Eosin-Y within the photopolymer solution, a volume of $10 \times 10 \times 10\ nm^3$ contains only four dye molecules. The same volume contains an average of 200 MDEA molecules and 6000 C=C double bonds. Considering this simple assessment, it appears that the limited reactant is the dye. The result is the curve in figure 14, showing that low irradiation powers (e.g. long irradiation times) are beneficial for polymerization.

The dye diffusion turns out to be important to describe the photopolymerization at the nanoscale. Although in

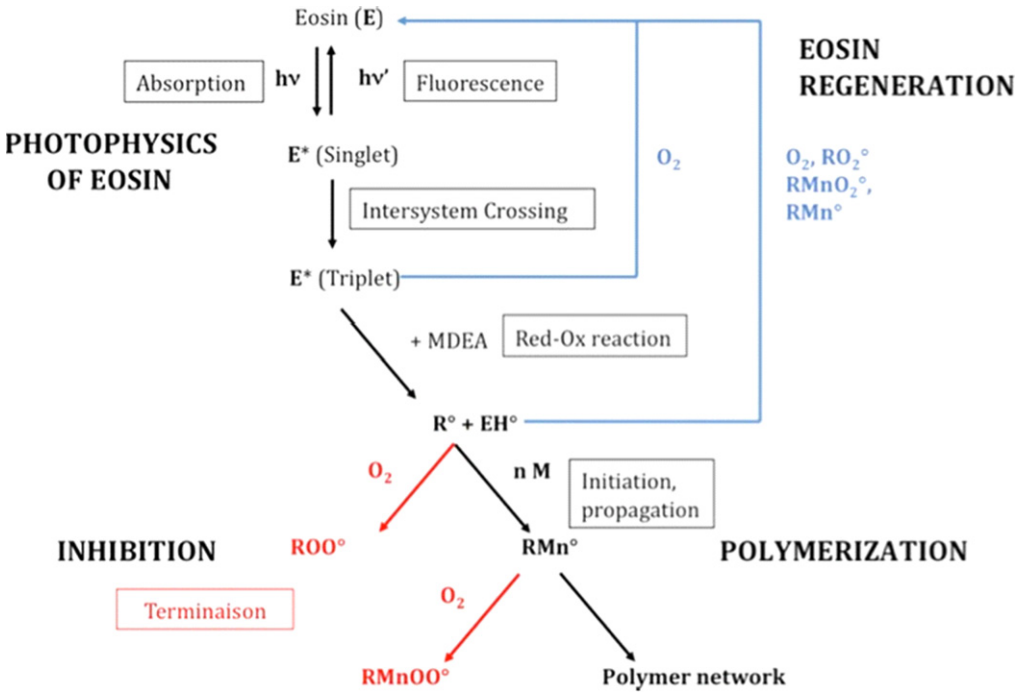

Figure 12. Scheme illustrating the photoinduced polymerization of the methacrylate monomer, the inhibition processes, and the Eosin-Y regeneration pathways. Reprinted with permission from [71]. Copyright 2011 American Chemical Society.

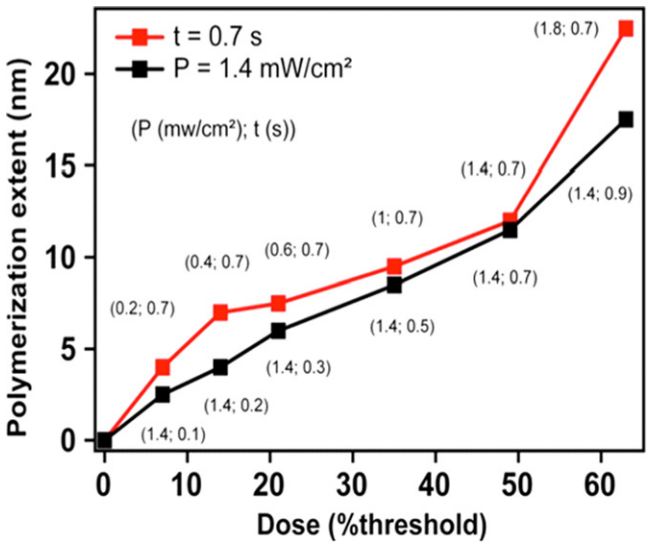

Figure 13. Evolution of the spatial extent of the near-field photopolymerization as a function of relative dose, at constant power (black curve) and constant irradiation time (red curve). Reprinted with permission from [71]. Copyright 2011 American Chemical Society.

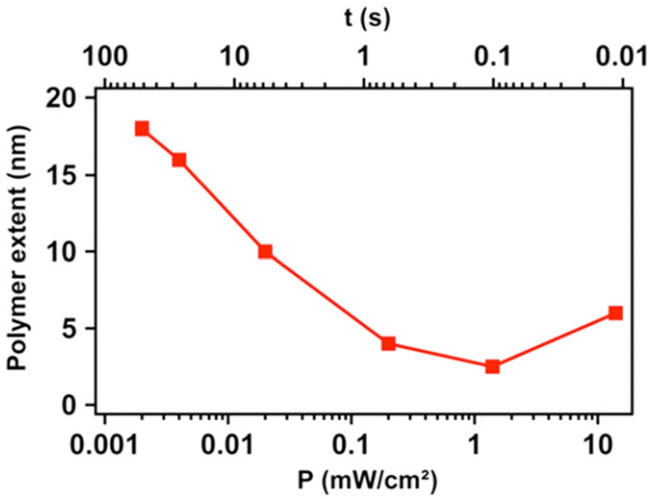

Figure 14. Influence of the incident power (bottom axis) and the exposure time (top axis) on the spatial extent of polymerization. The incident dose was set at 7% of the threshold dose. Reprinted with permission from [71]. Copyright 2011 American Chemical Society.

microscale photo-fabrication the dye diffusion is usually neglected, this parameter is of critical importance at the nanoscale. Dye diffusion in the monomer matrix is quite slow because of its high molecular weight and polarity. However, by reducing the scale of investigation and probing, it is possible to become sensitive to the dyes that diffuse in the irradiated volume. Furthermore, the diffusion process can be efficient since bleaching is negligible in the volume corresponding to the optically enhanced region. Low intensity corresponds to higher irradiation times, which certainly increases the probability of the dye to diffuse in the near-field nanoscale volume. This discussion is specific to the nanoscale and is linked to the extremely limited number of molecules: at the microscale, the average number of molecules present in the irradiation volume ($1000 \times 1000 \times 1000\ \text{nm}^3$) is greater by a factor of 10^6 and thus diffusion of the dye from the polymer droplet into the irradiated volume is not predominant. The limiting process at this length scale is the number of photons

absorbed by the photopolymer per second and hence, for a given dose, competitive processes such as inhibition by oxygen are more important.

5. Conclusion and perspectives

In this review, we have highlighted recent advances in plasmon-induced photopolymerization processes that create hybrid nanomaterials with modified optical properties. This is a highly multidisciplinary field requiring understanding of the complex range photochemical processes that impact the spatial features on the nanoscale hybrid nanostructures, as well as being motivated by complex interactions between molecules and metal nanostructures that produce novel optical effects. We have shown that plasmon-induced photopolymerization by metal nanoparticles produces important optical effects including anisotropic antenna behavior achieved with resonant interactions, as well as strong anisotropy in resonant effects, such as plasmon-enhanced emission processes.

Future work will be governed by advances in the ability to control the photopolymerization process at the nanoscale in order to optimize molecule–plasmon interactions for a particular application. For example, control of the type of chromophore interaction with plasmons, such as strong or weak coupling, requires precise control over the spacing of the chromophores from the metal surface. For enhancement of molecular or quantum dot radiative effects, efficient routes to spacing the target chromophores at 5 nm from the surface should be found [73]. Conversely, strong coupling would generally benefit from a much closer, yet precise distance, to optimize strong coupling effects [74]. Both strong and weak coupling interactions would benefit from control of the orientation the molecular transition dipoles in the evanescent field.

The use of plasmon-induced photopolymerization could further significantly impact nanooptics if the fabrication processes can be optimized. These include tunable nanoantennas with greater efficiencies, optical gain and lasing, and highly efficient nonlinear nanostructures. All of these aspects are critical for miniaturization of next-generation optical devices. Hybridization at the nanoscale represents a highly plausible route towards these opportunities because of the novel optical properties that only hybrid nanomaterials can provide.

Acknowledgments

The authors would like to thank current and former colleagues that are (or have been) involved in this project in different ways (fruitful discussion, samples, previous achievements, participation in measurements, etc): P-M Adam, A Bouhelier, F Charra, C Ecoffet, C Fiorini, D Gérard, D Gosztola, L Huang, H Ibn El Ahrach, P K Jain, S Kostcheev, S Marguet, Y Qi, R D Schaller, S Telitel, A Vial and R Vincent. The authors thank the Partner University Funds program (PUF 2010) for partially supporting this work. X Z thanks the China Scholarship Council (CSC). Use of the Center for Nanoscale Materials was supported by the US. Department of Energy, Office of Science, Office of Basic Energy Sciences, under Contract No. DE-AC02-06CH11357. This work is also supported by the French agency for research (ANR grant HAPPLE) and by European community FEDER fund and the Region Champagne-Ardenne: Grants HYN-NOV and NANO'MAT.

References

[1] Maier S A 2007 Plasmonics *Fundamental and Applications* (Berlin: Springer)
[2] Bachelot R, Zhou X, Plain J, Adam P M, Baudrion A L, Gray S K and Wiederrecht G P 2014 *Proc. of SPIE—The Int. Soc. Opti. Eng.* **9126** 91260Z
[3] Koenderink A F 2010 *Opt. Lett.* **35** 4208–10
[4] Curto A G, Volpe G, Taminiau T H, Kreuzer M P, Quidant R and Van Hulst N F 2010 *Science* **329** 930–3
[5] Willets K A and Van Duyne R P 2007 *Annu. Rev. Phys. Chem.* **58** 267–97
[6] Atwater H , A and Polman A 2010 *Nat. Mater.* **9** 205–13
[7] Chen H, Mig T, Wang L, Sun L D, Wang J and Yan C H 2010 *Nano Today* **5** 494–505
[8] Acimovic S S, Kreuzer M P, Gonzalez M U and Quidant R 2009 *ACS Nano* **3** 1231–7
[9] Dintinger J, Klein S, Bustos F, Barnes W L and Ebbesen T W 2005 *Phys. Rev.* B **71** 035424
[10] Baudrion A L, Perron A, Veltri A, Bouhelier A, Adam P M and Bachelot R 2013 *Nano Lett.* **13** 282–6
[11] Salomon A, Gordon R J, Prior Y, Seideman T and Sukharev M 2012 *Phys. Rev. Lett.* **109** 073002
[12] Drexhage K H 1970 *Sci. Am.* **222** 108
[13] Chance R R, Prock A and Silbey R 1978 *Adv. Chem. Phys.* **37** 1–65
[14] Pockrand I, Brillante A and Mobius D 1980 *Chem. Phys. Lett.* **69** 499–504
[15] Zhang J, Fu Y, Chowdury M H and Lakowicz J R 2007 *J. Phys. Chem.* C **111** 11784–92
[16] Ipe B I and Thomas K G 2004 *J. Phys. Chem.* B **108** 13265–72
[17] Jin S Y, DeMarco E, Pellin M J, Farha O K, Wiederrecht G P and Hupp J T 2013 *J. Phys. Chem. Lett.* **4** 3527–33
[18] Wiederrecht G P, Wurtz G A and Hranisavljevic J 2004 *Nano Lett.* **4** 2121
[19] Wu X H, Gray S K and Pelton M 2010 *Opt. Express* **18** 23633–45
[20] Wurtz G A, Evans P R, Hendren W, Atkinson R, Dickson W, Pollard R J, Zayats A V, Harrison W and Bower C 2007 *Nano Lett.* **7** 1297–303
[21] Shah R A, Scherer N F, Pelton M and Gray S K 2013 *Phys. Rev.* B **88** 075411
[22] Govorov A O, Bryant G W, Zhang W, Skeini T, Lee J, Kotov N A, Slocik J M and Naik R R 2006 *Nano Lett.* **6** 984–94
[23] Peng S, McMahon J M, Schatz G C, Gray S K and Sun Y G 2010 *Proc. Natl. Acad. Sci.* **107** 14530–4
[24] Pramod P, Soumya C C and Thomas K G 2011 *J. Phys. Chem. Lett.* **2** 775–81
[25] Mukherjee S, Libisch F, Large N, Newmann O, Brown L V, Cheng J, Lassiter J B, Carter E A, Nordlander P and Halas N J 2013 *Nano Lett.* **13** 240–7
[26] Ueno K and Misawa H 2011 *Photochem. Photobio.* A **221** 130–7

[27] Watanabe K, Menzel D, Nilius N and Freund H J 2006 *Chem. Rev.* **106** 4301–20
[28] Gao S, Ueno K and Misawa H 2011 *Acc. Chem. Res.* **44** 251–60
[29] Suh J Y, Kim C H, Zhou W, Huntington M D, Co D T, Wasielewski M R and Odom T W 2012 *Nano Lett.* **12** 5769–74
[30] Hasobe T, Imahori H, Kamat P V, Ahn T K, Kim S K, Kim D, Fujimoto A, Hirakawa T and Fukuzumi S 2004 *J. Am. Chem. Soc.* **127** 1216–28
[31] Zhang H, Govorov A O and Bryant G W 2006 *Phys. Rev. Lett.* **97** 146804
[32] Watanabe K, Menzel D, Nilius N and Freund H J 2006 *Chem. Rev.* **106** 4301–20
[33] Kamat P V 2002 *J. Phys. Chem.* B **106** 7729–44
[34] Chen C J and Osgood R M 1983 *Phys. Rev. Lett.* **150** 1705
[35] Ueno K and Misawa H 2013 *J. Photochem. Photobio. C: Photochem. Rev.* **15** 31–52
[36] Hubert C *et al* 2005 *Nano Lett.* **5** 615–9
[37] Bian L L, Kumar J, Kim D Y, Williams J and Tripathy S K 1988 *Appl. Phys. Lett.* **73** 1817–9
[38] Juan M L, Plain J, Bachelot R, Vial A, Royer P, Gray S K, Montgomery J M and Wiederrecht G P 2009 *J. Phys. Chem.* A **113** 4647–51
[39] Hubert C *et al* 2008 *J. Phys. Chem.* C **112** 4111–6
[40] Galarreta B C, Rupar I, Young A and Lagugne-Labarthet F 2011 *J. Phys. Chem.* C **115** 15318–23
[41] Tsuboi Y, Shimizu R, Shoji T and Kitamura N 2009 *J. Am. Chem. Soc.* **131** 12623–7
[42] Nishi H, Asahi T and Kobatake S 2011 *J. Phys. Chem.* C **115** 4564–70
[43] Nie Z and Kumacheva E 2008 *Nat. Mater.* **7** 277–90
[44] Scott T F, Kowalski B A, Sullivan A C, Bowman C N and McLeod R R 2009 *Science* **324** 913–7
[45] Li L, Gattass R R, Gershgoren E, Hwang H and Fourkas J T 2009 *Science* **324** 910–93
[46] Andrew T L, Tsai H Y and Menon R 2009 *Science* **324** 917–21
[47] Hell S W 2009 *Nat. Methods* **6** 24–32
[48] See (www.microchem.com/Prod-SU8_KMPR.htm)
[49] Srituravanich W, Fang N, Sun C, Luo Q and Zhang X 2004 *Nano Lett.* **4** 1085–8
[50] Srituravanich W, Durant S, Lee H, Sun C and Zhang X 2005 *J. Vac. Sci. Technol.* B **23** 2636–9
[51] Sundaramurthy A, Schuck P J, Conley N R, Fromm D P, Kino G S and Moerner W E 2006 *Nano Lett.* **6** 355–60
[52] Ueno K, Juodkazis S, Shibuya T, Yokota Y, Mizeikis V, Sasaki K and Misawa H 2008 *J. Am. Chem. Soc.* **130** 6928–9
[53] Deeb C *et al* 2010 *ACS Nano* **4** 4579–86
[54] Wiederrecht G P 2004 *EPJ-Appl. Phys.* **28** 3–18
[55] Douillard L, Charra F, Korczak Z, Bachelot R, Kostcheev S, Lerondel G, Adam P M and Royer P 2008 *Nano Lett.* **8** 935–8
[56] Kociak M and García de Abajo J 2012 *MRS Bull.* **37** 39–46
[57] Deeb C, Zhou X, Miller R, Gray S K, Marguet S, Plain J, Wiederrecht G P and Bachelot R 2012 *J. Phys. Chem.* C. **116** 24734–40
[58] Yi M, Zhang D, Wang P, Jiao X, Blair S, Wen X, Fu Q, Lu Y and Ming H 2011 *Plasmonics* **6** 515–9
[59] Sherry L J, Chang S-H, Schatz G C, Van Duyne R P, Wiley B J and Xia Y 2005 *Nano Lett.* **5** 2034–8
[60] Zhang S, Bao K, Halas N J, Xu H and Nordlander P 2011 *Nano Lett.* **11** 1657–63
[61] Scharte M, Porath R, Ohms T, Aeschlimann M, Krenn J R, Ditlbacher H, Aussenegg F R and Liebsch A 2001 *Appl. Phys.* B **3** 305–10
[62] Zhou X, Gérard D, Bouhelier A, Jain P K, Plain J, Soppera O, Royer P and Bachelot R 2011 *J. Phys. Chem. Lett.* **2** 7–11
[63] El Ahrach H I, Bachelot R, Vial A, Lerondel G, Plain J and Royer P 2007 *Phys. Rev. Lett.* **98** 107402
[64] Kinkhabwala A, Yu Z, Fan S, Avlasevich Y, Mullen K and Moerner W E 2009 *Nat. Photonics* **3** 654–7
[65] Noginov M A, Zhu G, Belgrave A M, Bakker R, Shalaev V M, Narimanov E, Stout S, Herz E, Suteewong T and Wiesner U 2009 *Nature* **460** 1110–3
[66] Zhou X *et al* 2014 *Appl. Phys. Lett.* **104** 023114
[67] Derom S, Vincent R, G Bouhelier A and Colas des Francs G 2012 *Europhys. Lett.* **98** 47008
[68] Espanet A, Dos Santos G, Ecoffet C and Lougnot D J 1999 *Appl. Surf. Sci.* **138-139** 87–92
[69] Decker C and Jenkins A D 1985 *Macromolecule* **18** 1241–4
[70] Fouassier J P and Chesneau E 1991 *Makromol. Chem.* **192** 245–60
[71] Deeb C, Ecoffet C, Bachelot R, Plain J, Bouhelier A and Soppera O 2011 *J. Am. Chem. Soc.* **133** 10535–42
[72] Soppera O, Jradi S and Lougnot D J 2008 *J. Polym. Sci.* A **46** 3783–94
[73] Jin S, DeMarco E, Pellin M J, Farha O K, Wiederrecht G P and Hupp J T 2013 *J. Phys. Chem. Lett.* **4** 3527
[74] Wu X, Gray S K and Pelton M 2010 *Opt. Express* **18** 23634